Effect of the spatial filtering and alignment error of hot-wire probes in a wall-bounded turbulent flow

IOP Publishing Measurement Science and Technology

Meas. Sci. Technol. **22** (2011) 105408 (10pp) doi:10.1088/0957-0233/22/10/105408

Effect of the spatial filtering and alignment error of hot-wire probes in a wall-bounded turbulent flow

A Segalini, A Cimarelli, J-D Rüedi, E De Angelis and A Talamelli

DIEM, Dipartimento di Ingegneria delle Costruzioni Meccaniche Nucleari Aeronautiche e di Metallurgia, Alma Mater Studiorum—Università di Bologna, Via Fontanelle 40, 47100 Forlì (FC), Italy

E-mail: antonio.segalini@unibo.it

Received 21 December 2010, in final form 19 June 2011
Published 2 September 2011
Online at stacks.iop.org/MST/22/105408

Abstract

The effort to describe velocity fluctuation distributions in wall-bounded turbulent flows has raised different questions concerning the accuracy of hot-wire measurement techniques close to the wall and more specifically the effect of spatial averaging resulting from the finite size of the wire. Here, an analytical model which describes the effect of the spatial filtering and misalignment of hot-wire probes on the main statistical moments in turbulent wall-bounded flows is presented. The model, which is based on the two-point velocity correlation function, shows that the filtering is directly related to the transverse Taylor micro-scale. By means of turbulent channel flow DNS data, the capacity of the model to accurately describe the probe response is established. At the same time, the filtering effect is appraised for different wire lengths and for a range of misalignment angles which can be expected from good experimental practice. Effects of the second-order terms in the model equations are also taken into account and discussed. In order to use the model in a practical situation, the Taylor micro-scale distribution at least should be provided. A simple scaling law based on classic turbulence theory is therefore introduced and finally employed to estimate the filtering effect for different wire lengths.

Keywords: wall-bounded turbulence, hot-wire anemometry, averaging, resolution

1. Introduction

Wall-bounded turbulence has been extensively investigated for more than a century but most fundamental questions tackled over the years still remain without a clear physical answer. Due to the complexity of the turbulence dynamics, most significant advances to date rely mainly on dimensional analysis, isotropy assumption and scaling laws based on simple physical arguments. The description of the mean stream-wise velocity profile is a good example of this methodology. Its description, in terms of inner and outer variables, is well established for the logarithmic region of the flow but the region closer to the wall still relies on *ad hoc* models surprisingly accurate for the little physics they contain. The relative ease to measure mean stream-wise velocity profiles with different experimental techniques provides reliable data to validate the theoretical models. The stream-wise velocity variance profile $\langle u'^2 \rangle (y)$, on the other hand, lacks a complete physical description and its scaling is not yet well understood, even if some attempts have been made [1, 2]. This problem is complicated by the difficulty to obtain reliable data of the turbulence intensity profile for large Reynolds numbers. While direct numerical simulations (DNS) offer well-resolved data at low Reynolds number only, most experimental data at higher Reynolds number suffer from different experimental problems, namely wall interference, positioning and resolution. The latter problem has been widely discussed in the literature [3–5] and even motivated the construction of new experimental facilities [3], which will allow the resolution of all turbulent scales in a high Reynolds number flow. The current lack of well-resolved data in the vicinity of the wall over a wide range of Reynolds number results in many speculations concerning the real value of $\langle u'^2 \rangle$ and the filtering effect of the sensors. This problem is even more significant when the sensors cannot

be oriented along a homogeneity direction of the flow, like for multiple velocity component measurements. In this case, even smaller sensors are required or *ad hoc* correction algorithms [6, 7] must be applied.

Single hot-wire anemometry is widely used when high-frequency measurements of the stream-wise velocity component close to the wall are needed. This technique offers excellent resolution in the wall-normal direction but a limited one in the span-wise direction due to the difficulty of building small-size sensors (even though micro-probes have recently been designed and developed at Princeton [8]). It is clear that the finite probe size acts as a spatial filter for the velocity fluctuations of span-wise scale comparable to the sensor size, affecting the velocity statistics. The span-wise filtering effect of a single wire probe was first investigated analytically by Frenkiel [9] under isotropic turbulent flow conditions. In turbulent wall-bounded flows, several experiments [10–13] and numerical simulations [14–16] have analyzed this effect. The results have been used to derive different empirical fits to correct the measured stream-wise velocity variance with special emphasis on the filtering of the near-wall peak.

Another effect, which to the authors' knowledge has not been discussed in the literature but is also related to the physical extension of the wire along the span-wise direction, is the effect of the probe misalignment with respect to the wall. This type of uncertainty increases typically when small home-built probes are used. In this case, for manufacturing reasons, the relative position between the wire and the probe support cannot be guaranteed. While optical alignment methods allow us to keep this error small, it is still not clear what is its impact on the measurement uncertainty.

The aim of this paper is to develop a simple analytical model which is capable of correctly reproducing the response of a finite-length sensor when it is positioned with a small angle relative to the wall. The paper is organized as follows: the theoretical model is developed in section 2. In section 3, the model predictions are estimated and compared with filtered DNS data and discussed also in view of some recently proposed correction procedures for wall-bounded turbulence measurements [17]. The issues of nonlinear filtering and probe angle are also presented and discussed. A practical implementation of the proposed model is then reported in section 4 where a simple scaling relationship, useful to provide the Taylor micro-scale, is proposed to estimate the filtering effect for different wire lengths in real experiments. Section 5 concludes this paper and summarizes the main outcomes.

2. The analytical model

A reference frame is defined with the x-axis aligned with the mean flow direction, while the y- and z-axes are normal and parallel to the wall, respectively. As schematically shown in figure 1, a wire of length L and diameter d is placed in the yz-plane with its center at $\mathbf{x_0} = (x_0, y_0, z_0)$ with an angle φ from the z-axis. A generic point along the wire is defined as $\mathbf{s} = \mathbf{x_0} + s\mathbf{w}$, where s ranges from $-L/2$ to $L/2$ and $\mathbf{w} = (0, \varphi, 1)$ is a tangential unitary

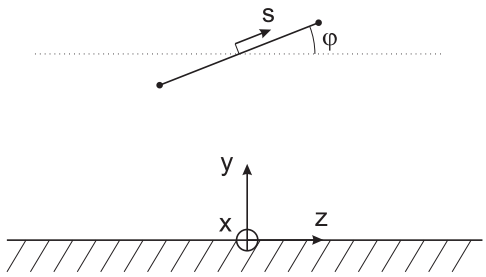

Figure 1. Reference frame.

vector assuming a small angle $\varphi \ll 1$ radiant, which is perfectly acceptable for the range of misalignment expected from good experimental practice. As notation, the real mean and standard deviation of the stream-wise velocity in $\mathbf{x_0}$ will be indicated with U_0 and $\langle u'^2\rangle_0^{1/2}$, respectively, where $\langle\cdot\rangle$ will be the ensemble average operator. Measured quantities will be denoted with the subscript m. Scaling of physical quantities with viscous variables (namely the friction velocity u_τ and kinematic viscosity ν) will be indicated with the conventional superscript +.

Hot-wire sensors are usually calibrated against a flow of known velocity magnitude and direction in order to associate an effective cooling velocity u_{eff} with a measured voltage $e_{\mathrm{w}}(t)$. It is assumed here that the wall-normal velocity v is small compared to the stream-wise velocity u (namely $v/u \ll 1$) and that the heat transfer toward probe supports and the wall is negligible. Under these assumptions, the cooling of the sensor mainly results from the stream-wise convective heat transfer and $u_{\mathrm{eff}} \approx u$. If the incoming flow is not homogeneous, the heat transfer along the wire is not uniform, with the consequence that the measured effective velocity becomes some integral average of the stream-wise velocities impinging the wire. Inspired by King's law, where the heat transfer $\dot{Q}$ is related to u_{eff}^n (i.e. $\dot{Q} \propto e_{\mathrm{w}}^2 \propto A + Bu_{\mathrm{eff}}^n$, where A, B and n are constants), the following nonlinear average is proposed to relate the instantaneous measured velocity $u_{\mathrm{m}}(t)$ to the local stream-wise velocity $u(\mathbf{s}, t)$ independently of the calibration chosen, which is expressed by the function $g[e_{\mathrm{w}}(t)]$:

$$u_{\mathrm{m}}(t) = g[e_{\mathrm{w}}(t)] = \left(\frac{1}{L}\int_{[-\frac{L}{2},\frac{L}{2}]} u^n(\mathbf{s}, t)\,\mathrm{d}s\right)^{1/n}. \qquad (1)$$

The exponent n accounts here for a nonlinear heat transfer process similar to King's law [18], for which $n \approx 0.5$ would be expected. In the special case of $n = 1$, the nonlinear average operator reduces simply to a linear top hat filter. In the following equations, the integration is always performed along the wire span $\left[-\frac{L}{2}, \frac{L}{2}\right]$, so such an integration will be indicated as $\int_P$.

The instantaneous stream-wise velocity is described using Reynolds decomposition,

$$u(\mathbf{s}, t) = \langle u\rangle(\mathbf{s}) + u'(\mathbf{s}, t), \qquad (2)$$

where the mean flow and the statistics of the fluctuating part are assumed to be statistically horizontally homogeneous, hence a function of y only, namely $\langle u\rangle(\mathbf{s}) = U(y)$ and

$\langle u'^2(\mathbf{s},t)\rangle = \langle u'^2\rangle(y)$. The mean measured velocity is obtained by averaging equation (1),

$$\langle u_\mathrm{m}\rangle = \left\langle \left(\frac{1}{L}\int_P u^n(\mathbf{s},t)\,\mathrm{d}s \right)^{1/n} \right\rangle, \tag{3}$$

where the velocity $u(\mathbf{s},t)$ can be substituted with the Reynolds decomposition (2) and where the mean term $U(y)$ can be replaced with a Taylor expansion

$$u(\mathbf{s},t) = U_0\left(1 + s\varphi\beta + s^2\varphi^2\theta + \frac{u'(\mathbf{s},t)}{U_0}\right) + \mathrm{O}(\varphi^3). \tag{4}$$

In equation (4), $\beta = \frac{1}{U_0}\left(\frac{\mathrm{d}\langle u\rangle}{\mathrm{d}y}\right)_{\mathbf{x_0}}$ is the slope parameter and $\theta = \frac{1}{2U_0}\left(\frac{\mathrm{d}^2\langle u\rangle}{\mathrm{d}y^2}\right)_{\mathbf{x_0}}$ is the curvature parameter.

In the following, it will be assumed that $u'/U_0 \ll 1$, which is a valid approximation outside the buffer layer but questionable inside it as the ratio of these two quantities rises up to 0.4 at the wall [11]. This assumption implies that, for small φ, $f(s) = s\varphi\beta + s^2\varphi^2\theta + u'/U_0 \ll 1$. The term inside the brackets of equation (3) is nonlinear for $n \neq 1$ and would add significant complexity to the following developments if used as such; hence, a simplification is introduced to express it through a Taylor expansion for small $f(s)$

$$\left[\frac{1}{L}\int_P (1+f(s))^n\,\mathrm{d}s\right]^{1/n} = 1 + \frac{1}{L}\int_P f(s)\mathrm{d}s + \frac{n-1}{2L}\left[\int_P f^2(s)\,\mathrm{d}s - \frac{1}{L}\left(\int_P f(s)\,\mathrm{d}s\right)^2\right] + \mathrm{O}(f^3). \tag{5}$$

By substituting expression (4) into equation (1), and by using expansion (5), it is possible to determine an expression for the instantaneous measured stream-wise velocity

$$\begin{aligned}\frac{u_m}{U_0} &= 1 + \frac{L^2}{12}\varphi^2\theta + \frac{1}{LU_0}\int_P u'(\mathbf{s},t)\,\mathrm{d}s \\ &+ \frac{n-1}{2LU_0}\left[\frac{1}{12}\varphi^2\beta^2U_0L^3 + \frac{1}{U_0}\int_P u'^2(\mathbf{s},t)\,\mathrm{d}s\right. \\ &+ 2\varphi\beta\int_P su'(\mathbf{s},t)\,\mathrm{d}s + 2\varphi^2\theta\int_P s^2u'(\mathbf{s},t)\,\mathrm{d}s \\ &- \frac{1}{LU_0}\int_P\int_P u'(\mathbf{s},t)u'(\mathbf{q},t)\,\mathrm{d}s\,\mathrm{d}q \\ &\left.- \frac{L^2}{6}\varphi^2\theta\int_P u'(\mathbf{s},t)\,\mathrm{d}s\right] + \mathrm{O}\left(\varphi^3, \frac{u'^3}{U_0^3}, \varphi\frac{u'^2}{U_0^2}\right).\end{aligned} \tag{6}$$

Finally, by averaging equation (6), the expression for the measured mean velocity is obtained

$$\begin{aligned}\frac{\langle u_\mathrm{m}\rangle}{U_0} &= 1 + \varphi^2\frac{L^2}{12}\left(\theta + \frac{n-1}{2}\beta^2\right) + \frac{n-1}{2LU_0^2}\left(\int_P \langle u'^2(\mathbf{s},t)\rangle\,\mathrm{d}s\right. \\ &\left.- \frac{1}{L}\int_P\langle u'(\mathbf{s},t)u'(\mathbf{q},t)\rangle\,\mathrm{d}s\,\mathrm{d}q\right) + \mathrm{O}\left(\varphi^4, \frac{u'^3}{U_0^3}, \varphi^2\frac{u'^2}{U_0^2}\right).\end{aligned} \tag{7}$$

This result clearly highlights that, if $n = 1$, the effect of the probe angle is related only to the velocity profile curvature, while an extra term related to the velocity profile slope appears otherwise due to nonlinear phenomena. The even exponent of the probe-angle correction is not surprising as the flow is assumed to be statistically span-wise homogeneous; hence, the error of the statistical quantities due to the probe angle must be an even function of φ. This expression also shows that velocity fluctuations only affect the mean measured velocity through the nonlinear filtering effect of the hot-wire. The standard deviation of the local velocity in equation (7) can be expressed with a procedure analogous to the one used for equation (4), namely

$$\langle u'^2(\mathbf{s},t)\rangle^{1/2} = \langle u'^2\rangle_0^{1/2}(1 + s\varphi\gamma + s^2\varphi^2\omega) + \mathrm{O}(\varphi^3), \tag{8}$$

with

$$\gamma = \frac{1}{\langle u'^2\rangle_0^{1/2}}\left(\frac{\mathrm{d}\langle u'^2\rangle^{1/2}}{\mathrm{d}y}\right)_{\mathbf{x_0}},$$

$$\omega = \frac{1}{2\langle u'^2\rangle_0^{1/2}}\left(\frac{\mathrm{d}^2\langle u'^2\rangle^{1/2}}{\mathrm{d}y^2}\right)_{\mathbf{x_0}}.$$

The two-point correlation $\langle u'(\mathbf{s},t)u'(\mathbf{q},t)\rangle$ can be re-expressed using the two-point correlation coefficient $\rho_{11}(\mathbf{s},\mathbf{q})$ defined as

$$\rho_{11}(\mathbf{s},\mathbf{q}) = \frac{\langle u'(\mathbf{s},t)u'(\mathbf{q},t)\rangle}{\sqrt{\langle u'^2(\mathbf{s},t)\rangle}\sqrt{\langle u'^2(\mathbf{q},t)\rangle}}, \tag{9}$$

which can be simplified with a change of variables $(\mathbf{s_c},\mathbf{r}) = \left(\mathbf{x_0} + \frac{s+q}{2}\mathbf{w}, (s-q)\mathbf{w}\right)$, where $\mathbf{s_c}$ and $\mathbf{r}$ are the middle point and vector between $\mathbf{s}$ and $\mathbf{q}$, respectively. A polynomial expression of ρ_{11} can be developed using a Taylor expansion around the point $(\mathbf{x_0},\mathbf{0})$ with constraints for

- boundedness: $|\rho_{11}(\mathbf{s_c},\mathbf{r})| \leqslant 1\ \forall\,(\mathbf{s_c},\mathbf{r})$,
- symmetry: $\rho_{11}(\mathbf{s_c},\mathbf{r}) = \rho_{11}(\mathbf{s_c},-\mathbf{r})\ \forall(\mathbf{s_c},\mathbf{r})$,
- locality: $\rho_{11}(\mathbf{s_c},\mathbf{0}) = 1\ \forall\mathbf{s_c}$.

The only polynomial satisfying these requirements up to the fourth order, in the proximity of the wire middle point, is

$$\begin{aligned}\rho_{11}(\mathbf{s_c},\mathbf{r}) &= 1 + \sum_{i,j}A_{ij}r_ir_j + \sum_{i,j,k}B_{ij,k}r_ir_j(\mathbf{s_c}-\mathbf{x_0})_k \\ &+ \sum_{i,j,k,g}C_{ij,km}r_ir_j(\mathbf{s_c}-\mathbf{x_0})_k(\mathbf{s_c}-\mathbf{x_0})_g \\ &+ \sum_{i,j,k,g}D_{ijkm}r_ir_jr_kr_g,\end{aligned} \tag{10}$$

where

$$\begin{aligned}A_{ij} &= \frac{1}{2}\left(\frac{\partial^2\rho_{11}}{\partial r_i\partial r_j}\right)_{\mathbf{x_0}}, \\ C_{ij,kg} &= \frac{1}{24}\left(\frac{\partial^4\rho_{11}}{\partial r_i\partial r_j\partial s_{m,k}\partial s_{m,g}}\right)_{\mathbf{x_0}} \\ B_{ij,k} &= \frac{1}{6}\left(\frac{\partial^3\rho_{11}}{\partial r_i\partial r_j\partial s_{m,k}}\right)_{\mathbf{x_0}}, \\ D_{ijkg} &= \frac{1}{24}\left(\frac{\partial^4\rho_{11}}{\partial r_i\partial r_j\partial r_k\partial r_g}\right)_{\mathbf{x_0}}.\end{aligned} \tag{11}$$

These coefficients can be simplified considering the following three points: (1) there is no x-dependence in the present formulation, (2) all derivatives in $s_{m,3}$ are equal to zero due to the homogeneity in the z-direction and (3) all the odd derivatives in r_3 are equal to zero due to the symmetry

of the turbulent field relative to the xy-plane. With these simplifications, it is now possible to express the two-point correlation coefficient as

$$\rho_{11}(\mathbf{s},\mathbf{q}) \approx 1 + (s-q)^2[\Gamma_2 + \Gamma_3(s+q) + \Gamma_{4,1}(s+q)^2 + \Gamma_{4,2}(s-q)^2], \tag{12}$$

where

$$\Gamma_2 = A_{33} + A_{22}\varphi^2 \qquad \Gamma_{4,1} = \frac{3\varphi^2}{2}(C_{33,22} + C_{22,22}\varphi^2)$$
$$\Gamma_3 = \frac{3\varphi}{2}(B_{33,2} + B_{22,2}\varphi^2),$$
$$\Gamma_{4,2} = D_{3333} + 6D_{3322}\varphi^2 + D_{2222}\varphi^4. \tag{13}$$

The coefficient Γ_2 must be negative everywhere to ensure boundedness and is related to the transverse Taylor micro-scale λ_g:

$$\Gamma_2 = A_{33} + \mathrm{O}(\varphi^2) = \frac{1}{2}\left(\frac{\partial^2\rho_{11}}{\partial r_3^2}\right) + \mathrm{O}(\varphi^2) = -\frac{1}{\lambda_g^2} + \mathrm{O}(\varphi^2). \tag{14}$$

As will be seen in the following, the coefficient A_{33}, or equivalently the transverse Taylor micro-scale λ_g, plays a leading role in the filtering properties [9]; hence, special attention is devoted to it in section 4 and in the appendix where a practical way to determine the Taylor micro-scale in the equilibrium region is described.

Recalling equation (7), it is now possible to express the integrals with equations (8), (9) and (12), obtaining

$$\frac{\langle u_m\rangle}{U_0} = 1 + \varphi^2\frac{L^2}{12}\left(\theta + \frac{n-1}{2}\beta^2\right) - \frac{n-1}{60}\frac{\langle u'^2\rangle_0}{U_0^2}L^2(5A_{33} + 2D_{3333}L^2) + \mathrm{O}\left(\varphi^4, \frac{u'^3}{U_0^3}, \varphi^2\frac{u'^2}{U_0^2}\right). \tag{15}$$

As already stated, the probe-angle correction is only related to the mean velocity profile through β and θ, while the nonlinear filtering effects influence the measured mean velocity, regardless of the probe angle, as observed in [12].

An expression for the measured stream-wise velocity variance can now be obtained using equations (6)–(9) and (12) as

$$\frac{\langle u_m'^2\rangle}{\langle u'^2\rangle_0} = 1 + G_1 + \varphi^2 G_2 + (n-1)L^2\varphi^2\left[-\frac{\theta}{6} - \frac{\theta}{6}G_1 + (n-1)\beta^2L^2G_3 + 2\beta G_4 + 2\theta G_5\right] + \mathrm{O}\left(\varphi^4, \frac{u'^3}{U_0^3}\right), \tag{16}$$

where

$$G_1 = \frac{1}{6}A_{33}L^2 + \frac{1}{15}D_{3333}L^4$$
$$G_2 = \frac{L^2}{2520}[420(A_{22}+\omega) + 7L^2(6C_{33,22} + 144D_{3322} + 6\gamma B_{33,2} + 14\omega A_{33} - 5\gamma^2A_{33}) + 3L^4D_{3333}(16\omega - 7\gamma^2)]$$
$$G_3 = -\frac{1}{360}(5A_{33} + 3D_{3333}L^2) \tag{17}$$
$$G_4 = \frac{1}{2520}[210\gamma + 7L^2(3B_{33,2} + 2\gamma A_{33}) + 3L^4\gamma D_{3333}]$$
$$G_5 = \frac{1}{2520}(210 + 49L^2A_{33} + 24L^4D_{3333}).$$

It can be seen from equations (16) and (17) that the term G_1 is related to the characteristics of the two-point correlation in the span-wise direction and is independent of the probe angle. The term G_2, on the other hand, is related to the effect of the probe angle only, while all other terms are related to both nonlinear filtering and probe-angle effects.

For $\varphi = 0$, equation (16) simplifies drastically and, only for $n = 1$, extra terms of ρ_{11} can be included to increase the application range up to the $(2N)$th order,

$$\frac{\langle u_m'^2\rangle}{\langle u'^2\rangle_0} = 1 - \frac{L^2}{6\lambda_g^2} + \sum_{i=2}^{N}\frac{2L^{2i}}{(2i+2)!}\frac{\partial^{2i}\rho_{11}}{\partial r_z^{2i}}, \tag{18}$$

which is similar to the relation proposed by Frenkiel [9] for isotropic conditions and linear filtering. The validity of the variance correction factor (18) can be extended to larger values of L^+ by increasing the number of terms in the expansion of ρ_{11}, but the divergence of the polynomial expansion gets sharper; hence, many high-order derivatives must be included for a limited improvement only.

3. Filtering effect and model validation

3.1. Data set

The model presented in section 2 is tested using a channel flow DNS. Since in this case the Taylor micro-scale and the derivatives of ρ_{11} are evaluated directly from the DNS data, the results obtained in this section represent only an appraisal of the capacity of the model to estimate the probe filtering and the effect of a wrong probe alignment in the flow. The simulation was performed on a channel with half height h at $Re_\tau = u_\tau h/\nu = 550$. The computational domain is $(L_x, L_y, L_z) = (8\pi h, 2h, 4\pi h)$ with $1024 \times 257 \times 1024$ grid points, respectively, corresponding to a resolution in wall units in the homogeneous directions of $\Delta x^+ = 13.49$ and $\Delta z^+ = 6.74$. In the wall-normal direction, the points are distributed with a cosine law with grid steps of $\Delta y^+ = 0.04$ close to the wall and $\Delta y^+ = 6.75$ at the channel centerline. The simulation was carried out with a pseudo-spectral code, which is fully described in [19]. The predictions of the present model are assessed with filtered DNS data with an integral average operator based on Simpson's integration method. For the tilted wire, the integration is performed along an inclined path, where the instantaneous stream-wise velocity is interpolated using a planar cubic spline. Finally, the derivatives of the two-point correlation function ρ_{11} (including the transverse Taylor micro-scale λ_g) are estimated using a second-order-accurate centered finite-difference scheme.

In the following, three different viscous-scaled wire lengths, L^+, will be used, namely 13.5, 27 and 40.5. They correspond, in the simulated flow field, to probes which have a physical dimension close to real ones. While the first

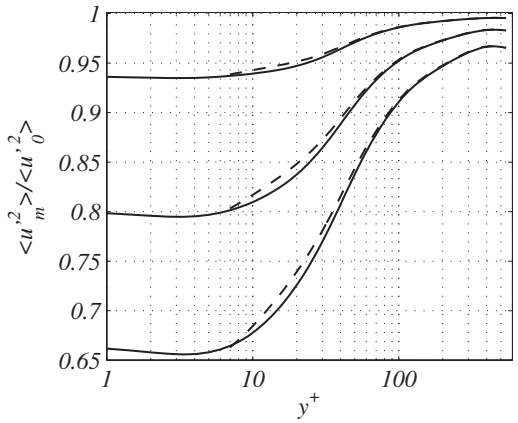

Figure 2. Effect of the nonlinear filtering on the measured variance of the stream-wise velocity for $\varphi = 0$ at $Re_\tau = 550$. From top to bottom: $L^+ = 13.5$, $L^+ = 27$ and $L^+ = 40.5$. (——) linearly filtered DNS data, (– – –) nonlinearly filtered DNS data with $n = 0.5$.

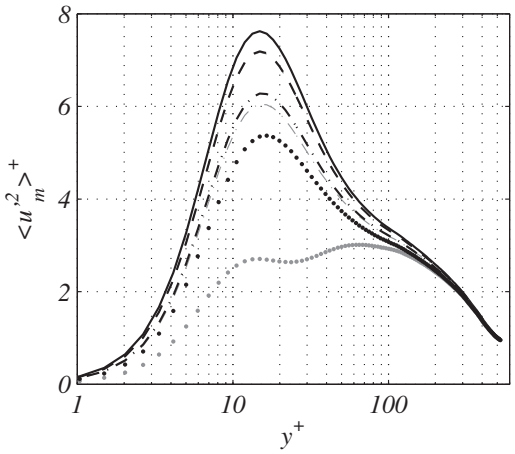

Figure 3. Filtered $\langle u'^2_m \rangle^+$ distribution for different wire lengths L^+ at $Re_\tau = 550$ and $\varphi = 0$. (——) no filter, (– – –) $L^+ = 13.5$, (— · —) $L^+ = 27$, (· · · · · ·) $L^+ = 40.5$. The black lines represent DNS filtered data, while the gray lines represent the predictions of equation (18) with $N = 3$.

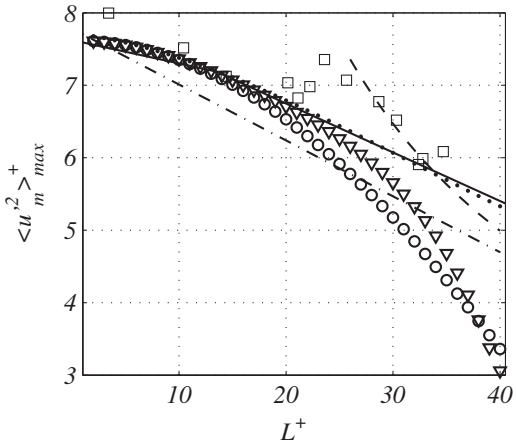

Figure 4. Effect of the wire length L^+ on the maximum measured value of $\langle u'^2_m \rangle^+$ for (——) filtered DNS data at $Re_\tau = 550$, (○) equation (18) (second derivative only), (▽) equation (18) ($N = 3$), (□) data from Johansson and Alfredsson [11] ($Re_\tau = 1000$–2600), (– – –) Ligrani and Bradshaw [10] ($Re_\tau = 930$), (— · —) Hutchins *et al* [15] ($Re_\tau = 316$–25000) and (· · · · · ·) Chin *et al* [16] ($Re_\tau = 934$).

two are generally thought to give limited spatial resolution effects in the experimental practice, the last one is considered a measurement condition that will sensibly affect the quality of the measured velocity variance and of the higher order moments.

3.2. Spatial resolution with $\varphi = 0$

In this section, we investigate the capacity of the proposed model to reproduce the filtering effect when the probe is positioned correctly in the flow. In the special case of $\varphi = 0$, nonlinear filtering effects disappear from equation (16), and equation (18) can be directly applied to estimate the effect of the wire length on the measured variance. The third-order moment terms that have been neglected in expansion (16) do not play a significant role compared to the spatial averaging effect as demonstrated in figure 2 where the comparison between linear and nonlinear filtered DNS data with $\varphi = 0$ shows little difference.

The effect of the wire length calculated from filtered DNS data and as predicted by the model of the stream-wise velocity variance from equation (18) with $N = 3$ (i.e. by using the DNS-computed derivatives of the two-point correlation function up to the sixth order), scaled with the squared friction velocity u_τ^2, is shown in figure 3 for $Re_\tau = 550$ and $\varphi = 0$. It appears clearly that the length of the hot-wire acts as a filtering function on the velocity fluctuations and that this effect increases toward the wall, where the length of the most energetic eddies decreases rapidly. The agreement between the DNS filtered data and the model is excellent at $L^+ = 13.5$ where the two distributions overlap, but the accuracy of the model quickly decreases for larger L^+, especially in the proximity of the near-wall peak due to the limited order of the Taylor expansion of the two-point correlation ρ_{11}, whose accuracy decreases as L^+/λ_g^+ increases.

The effect of the wire length on the measured maximum variance $\langle u'^2_m \rangle^+_{max}$ is shown in figure 4 where filtered DNS data at $Re_\tau = 550$ are compared with the present model together with empirical fits proposed by different authors [10, 15], as well as with the collection of experimental data of Johansson and Alfredsson [20]. Re_τ for boundary layers has been computed as $Re_\tau = u_\tau \delta_{99}/\nu$. The results of equation (18) are reported here without the summation term (only the Taylor micro-scale is considered) or with $N = 3$ where the Taylor micro-scale and the derivatives of ρ_{11} up to the sixth order are included. This simplification is important from an experimental point of view as the difficulty of measuring such derivatives increases significantly with their order. The agreement between the empirical fits, DNS filtered data and experimental measurements is fair considering the different Re_τ of the data presented here.

The formula proposed by Chin *et al* [16] follows DNS data remarkably well, since it has been obtained by fitting filtered data at $Re_\tau = 934$ which is close to that of the present DNS.

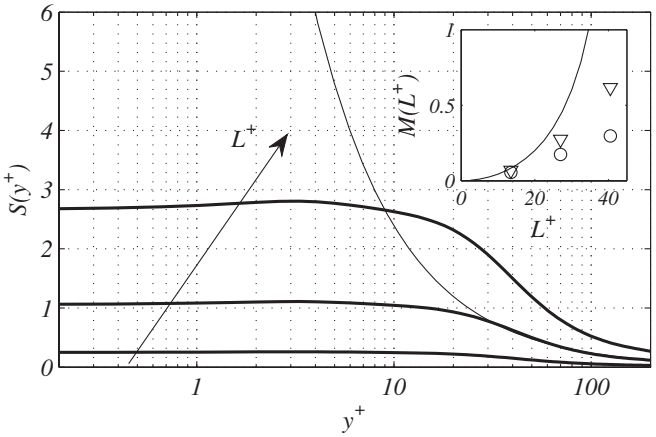

Figure 5. Filtering envelopes obtained from equation (20) fixing the distance from the wall y^+ (inset) and the wire length L^+ (main plot). The three curves in the main plot have been obtained fixing $L^+ = 7$, $L^+ = 14$ and $L^+ = 21$ in equation (20) normalizing the curves so that the value for $L^+ = 14$ is equal to 1 when y^+ is at the maximum of the velocity fluctuation. The line in the inset is the attenuation factor obtained by $\tilde{F}_2$ for y^+ at the maximum of the velocity fluctuation, while the symbols have been obtained extrapolating the attenuation factor from the curves in figure 3 using the DNS data at $Re_\tau = 550$. The circles represent the filtered DNS, while the triangles represent the analytical model with $N = 3$.

It is worth pointing out how well the correction based only on the transverse Taylor micro-scale

$$\frac{\langle u_{\mathrm{m}}'^2\rangle^+}{\langle u'^2\rangle_0^+} = 1 - \frac{(L^+)^2}{6\left(\lambda_{\mathrm{g}}^+\right)^2} = F_2(L^+, y^+) \tag{19}$$

manages to recover analytically the quadratic behavior of the filtered DNS for small L^+. The range of agreement increases when correction (18) with $N = 3$ is adopted. Following the same line of reasoning, it is also possible to show that equation (19) alone is able to reproduce qualitatively the fitting recently proposed by Smits *et al* [17] to correct measurements affected by spatial filtering in turbulent boundary layers. Namely, in the above-mentioned contribution, the authors propose a fitting law for the following attenuation factor:

$$\frac{\langle u'^2\rangle_0^+ - \langle u_{\mathrm{m}}'^2\rangle^+}{\langle u_{\mathrm{m}}'^2\rangle^+} = \tilde{F}_2(L^+, y^+) = M(L^+)S(y^+), \tag{20}$$

where $\tilde{F}_2(L^+, y^+)$ is easily related to $F_2(L^+, y^+)$ as

$$\tilde{F}_2(L^+, y^+) = \frac{1}{F_2(L^+, y^+)} - 1. \tag{21}$$

In equation (20), the filtering effect is expressed as the product of two different functions, M and S, depending only on L^+ and y^+, respectively. By using the analytic expression (21) for $F_2(L^+, y^+)$, it is possible to obtain in a closed form the fitting curves at least for small values of L^+. In detail, the plots for $M(L^+)$ and $S(y^+)$ in figure 5 are obtained fixing the values of L^+ and y^+. In the inset of the figure, the values of $M(L^+)$ are obtained as the values of the attenuation factor for the wall normal location where $\langle u'^2\rangle_0^+$ is maximum. Namely, the curve represents the analytic expression obtained via (20), while the symbols are extrapolated from the plots in figure 3. It appears clearly that the analytical small L^+ behavior is approached by the filtered data.

In the main plot of figure 5, the behavior of $S(y^+)$ is instead reported for three different values of L^+. The absolute values in the curves are arbitrary and depend on the choices made for the splitting. In this case, the normalization is such that only one, the middle one, has the property as in [17], i.e. it is equal to 1 when y^+ is at the maximum of the velocity fluctuation. It is remarkable to observe that, for the small values of L^+ chosen, when (20) is approximately valid, the structure of the filtering envelope S varying with the distance from the wall y^+ is fully captured just by the behavior of the transversal Taylor micro-scale. In particular, both the constant value close to the wall and the filtering effect further away, which decrease inversely with the distance from the wall, are related to the shape of λ_{g}. Moreover, it is interesting to note that the latter behavior, in the equilibrium layer, can be expected just assuming the theoretical prescription of λ_{g} as obtained in the appendix.

3.3. Probe alignment

The effects of the probe alignment on the mean streamwise component are shown in figure 6 for different values of n (1 and 0.5), probe angles φ (5° and 15°) and wire lengths L^+ (13.5 and 27). Note that the equations in section 2 have been developed with φ expressed in radians, while in the text and in the figure captions, it is expressed in degrees. The smallest angle φ is of the order of the alignment accuracy that can be manually achieved, while the largest one is shown here to demonstrate that significant deviations may be observed only at very high probe angles, where the assumption of small φ starts to be questionable. The curves begin at a wall distance corresponding to the lowest theoretically reachable position at the center of the sensor, namely $y^+ = L^+/2 \sin\varphi$, without considering any parts of the probe other than the sensing element itself. It is clear that the effective minimum sensor distance from the wall depends on the flow conditions and is likely to be significantly higher. In the figures, the model predictions, according to equation (15), are presented together with the filtered DNS results. The figures show clearly that for the measured mean velocity, the agreement is good almost everywhere. As expected, far from the wall, the measured value is almost unaffected by the alignment error. However, once the wall is approached, it starts to decrease, depending on L^+, φ and n. As expected, increasing the wire length or the probe angle also increases the attenuation of the mean velocity. Moreover, the attenuation is several times higher with $n = 0.5$ (nonlinear filtering) than with $n = 1$ (linear filtering) underlining the importance of accounting for nonlinear effects when evaluating probe-angle effects and pointing out the possible consequences on real hot-wire anemometer response.

A larger effect of the probe alignment can be seen in the velocity variance distribution presented in figure 7. The model prediction, in this case equation (16), appears to be slightly shifted, especially for $L^+ = 27$. This phenomenon is related to the expansion of the two-point correlation function,

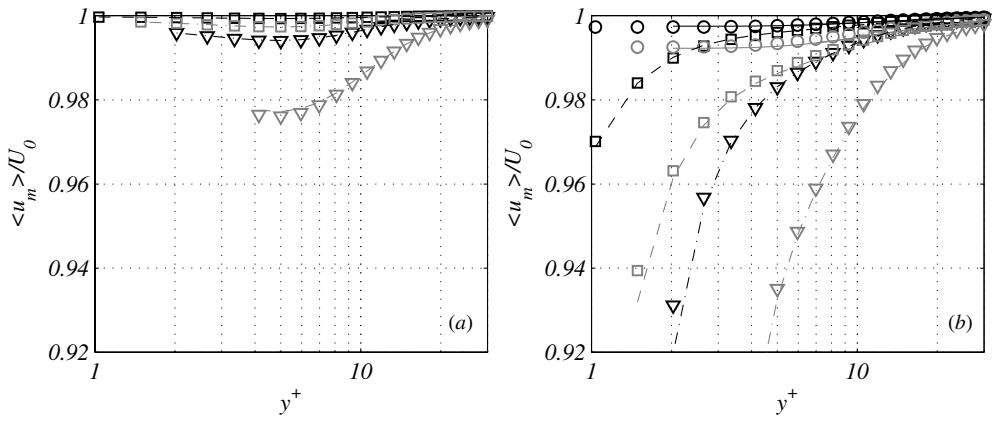

Figure 6. Relative error of the measured mean stream-wise velocity component for different probe lengths and positioning angles: (*a*) linear filtering, $n = 1$, and (*b*) nonlinear filtering, $n = 0.5$; (black symbols and lines) $L^+ = 13.5$ (gray symbols and lines), $L^+ = 27$ (gray). Filtered DNS data at $\varphi = 0$ (——), $\varphi = 5^\circ$ (– – –) and $\varphi = 15^\circ$ (— · —) and results from equation (15); at $\varphi = 0$ (○), $\varphi = 5^\circ$ (□) and $\varphi = 15^\circ$ (▽).

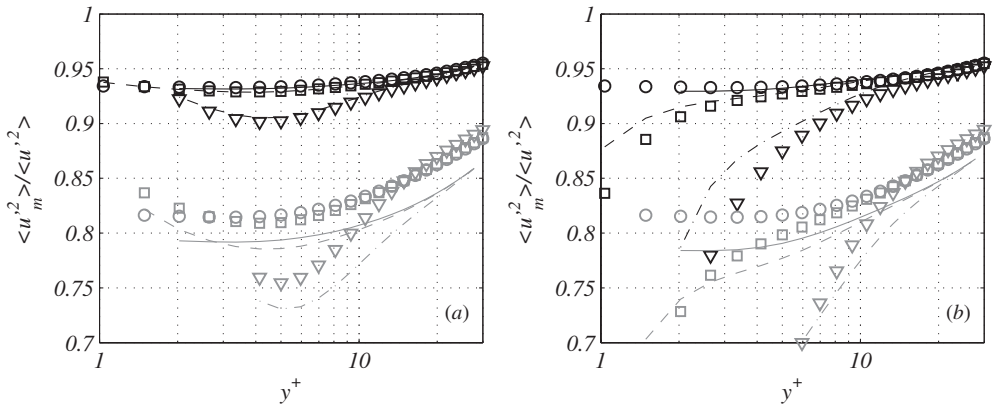

Figure 7. Relative error in the measured stream-wise velocity variance for different probe lengths and positioning angles: (*a*) linear filtering, $n = 1$, and (*b*) nonlinear filtering, $n = 0.5$; (black symbols and lines) $L^+ = 13.5$ (gray symbols and lines), $L^+ = 27$ (gray). Filtered DNS data at $\varphi = 0$ (——), $\varphi = 5^\circ$ (– – –) and $\varphi = 15^\circ$ (— · —) and results from equation (16); at $\varphi = 0$ (○), $\varphi = 5^\circ$ (□) and $\varphi = 15^\circ$ (▽).

which here is limited to the fourth order only. Better results could be obtained by extending this expansion toward higher order terms but adding significant complexity to the model. No significant alignment effect can be detected for a realistic probe angle $\varphi = 5^\circ$ for $y^+ > 20$ and the main error affecting the variance remains the wire length.

A comparison between figures 6 and 7 shows that nonlinear effects influence primarily the measured mean value. The curves show that the reduction is limited to about 1% of the local mean velocity for $L^+ \approx 30$ when $\varphi = 0$. This decrease has been already observed experimentally [12] inside the buffer region of turbulent boundary layers, in agreement with our DNS filtered data and theoretical predictions. Therefore, it can be concluded that nonlinear effects alone do not have serious consequences in the mean velocity; however, they become a serious source of error if coupled with a probe misalignment angle. As far as the variance behavior is concerned, both linear and nonlinear filtering appear to give the same trend. This agrees with the physical intuition that far from the wall, the mean velocity gradients are small as well as the local turbulence intensity, making $f(s)$ very small in equation (5). The nonlinearities will contribute to increase again the attenuation of the measured value, with an increasing effect as the wall is approached. Again, the trend predicted by the present model is confirmed by DNS data filtered along an inclined line but with a small offset due to the truncation error of the Taylor expansion of the two-point correlation coefficient.

4. Application of the model in wall-bounded turbulence experiments

In the experimental practice, the transverse Taylor micro-scale is a quantity which is not known *a priori* and is not likely to be accurately measured especially close to the wall. Several techniques can be used for this purpose (see for instance [21–24]). Here, in order to provide an estimation of the hot-wire spatial resolution error, a simple scaling law based on classical turbulence theory, which allows us to obtain a more reliable experimental evaluation of the transverse micro-scale, is proposed. The analytical development and the details of the scaling used are presented in the appendix. The advantage of the proposed relationship (namely $\lambda_g^+ = A\,(\kappa y^+)^{1/2}$) is that the constant A does not change with y^+ (at least in the equilibrium region) and therefore it must be found only once. Since the Taylor micro-scale is expected to grow monotonically with the wall distance, it is then suggested to estimate such a scale

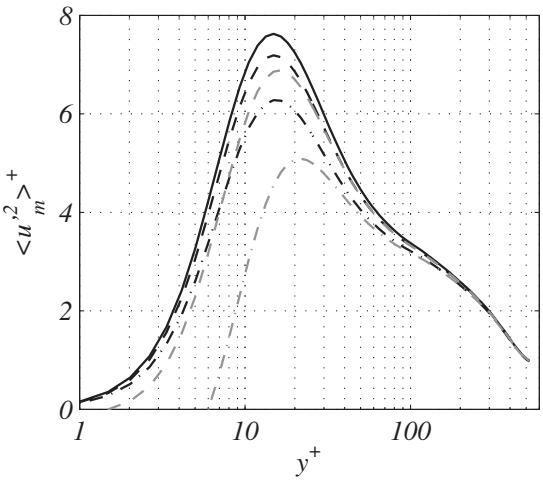

Figure 8. $\langle u_m'^2 \rangle^+$ distribution for different wire lengths L^+ at $Re_\tau = 550$. (——) no filter, (– – –) $L^+ = 13.5$, (— · —) $L^+ = 27$. The Taylor micro-scale is calculated from the numerical simulation (black lines) and estimated with the proposed scaling $\lambda_g^+ \propto (\kappa y^+)^{1/2}$ (gray lines).

close to the edge of the equilibrium part of the boundary layer, where the ratio L/λ_g is smaller allowing an easier experimental evaluation of the transverse micro-scale (for instance, by measuring the correlation function by means of two single standard hot-wires). The measured λ_g at the known height y^+ can then be used to practically determine A and to obtain λ_g in the whole equilibrium region.

In order to validate this procedure, the results are compared with filtered DNS data in figure 8. The coefficient $A\sqrt{\kappa}$ has been fitted with the known λ_g from our DNS data in the range $80 < y^+ < Re_\tau/5$. The good agreement between the two formulations for $y^+ > 40$ underlines that the proposed scaling is appropriate even for a distance below the logarithmic region of wall-bounded turbulent flows. These results show that it is possible to obtain an *a priori* estimation of the hot-wire spatial resolution error in the whole logarithmic layer, once the coefficient A is determined. It must be pointed out that the procedure proposed to estimate the Taylor micro-scale and therefore, the results reported in figure 8, refer to moderate Reynolds number flows. However, since relation (A.3) assumes the presence of an equilibrium region and of a small-scale isotropic recovery, it is expected that for larger Reynolds number flows such as those usually reproduced in experiments, the quality and the extension of the proposed scaling should increase.

5. Conclusions

An analytical model has been developed to describe the error of the mean and variance of the stream-wise velocity component when measured with a hot-wire sensor of finite length and with small misalignment angles relative to the wall. The model is based on an expansion of the velocity around the center of the probe and turns out to depend only on the derivatives of the transverse correlation function, and mainly on the transverse Taylor micro-scale. The model is found to be accurate up to a sensor length of about $L^+ \approx 25$ due to the limited accuracy of the Taylor expansion of the transverse two-point velocity correlation function. It is shown that the sensor length is the main source of error and that nonlinear filtering effects, resulting from a real hot-wire response, are limited to $y^+ < 20$ and are only important when combined with a sensor misalignment angle. This suggests that considering more sophisticated heat transfer corrections along the wire will not modify significantly the accuracy of the system and that linear filtering can be assumed for most cases.

The framework presented here provides new physical insight on the different parameters affecting the finite sensor size averaging process, which will be useful for the development of new correction tools based on physical flow properties. The model requires to know the transverse Taylor micro-scale and high-order derivatives of the transverse correlation function, which are not easy to measure in practice.

In order to use the model in practical situations, the Taylor micro-scale distribution should be provided. A simple scaling law based on classic turbulence theory is introduced and employed to estimate the filtering effect for different wire lengths. It is interesting to note that, since λ_g^+ increases also with the Reynolds number, the averaging effect at a constant y^+ also slightly decreases for increasing Re_τ, in agreement with the observations of Monkewitz *et al* [13].

Acknowledgments

The authors wish to acknowledge the support of the Italian Ministry of Research MIUR under PRIN08 grant and of the Region Emilia Romagna under the CIPE grant. The DNS was performed on a computing time grant provided by CASPUR.

Appendix

It is well known that in isotropic turbulence, the scale λ_g can be related to the Kolmogorov scale η in the form

$$\lambda_g = \sqrt{10}\eta^{2/3} L_s^{1/3}, \tag{A.1}$$

where L_s is a length scale characterizing the large eddies [25]. Even if wall turbulence is an intrinsically anisotropic and inhomogeneous phenomenon, isotropic recovery at the small scales in the logarithmic and bulk region is expected, at least for a large Reynolds number [26, 27]. For that reason, scaling behavior similar to equation (A.1) should hold. According to the classical theory, the logarithmic layer is an equilibrium region where turbulent production and dissipation balance. With this assumption and since the mean shear S can be written as $S \approx u_\tau/(\kappa y)$, it is possible to find that the local dissipation $\langle \epsilon \rangle$ can be estimated as $\langle \epsilon \rangle = u_\tau^3/(\kappa y)$, where κ is the Kármán constant. Assuming this scaling for the dissipation, the Kolmogorov scale $\eta = (\nu^3/\langle \epsilon \rangle)^{1/4}$ is expected to scale with the wall distance as $\eta^+ \propto (\kappa y^+)^{1/4}$, while the shear scale $L_s = (\langle \epsilon \rangle / S^3)^{1/2}$, which can be considered as the length scale characterizing the large eddies, is expected to scale with the wall distance as $L_s^+ \propto (\kappa y^+)$ [21]. Substituting these two

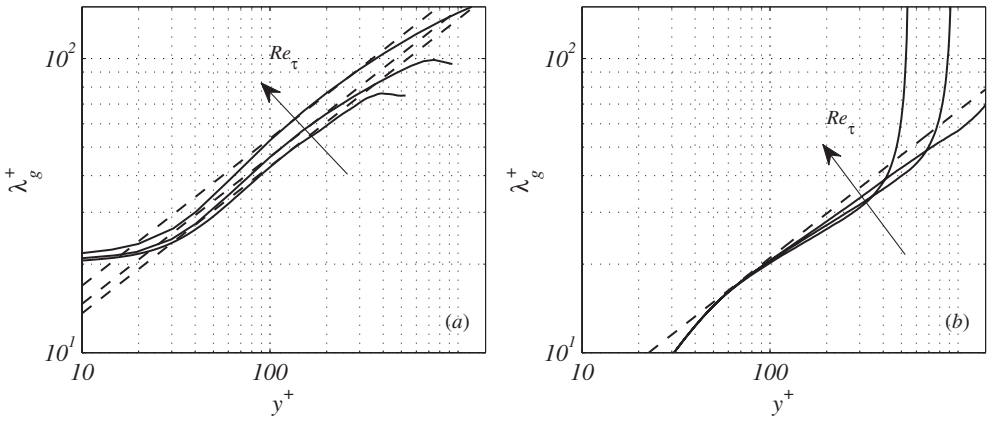

Figure A1. (*a*) Transverse Taylor micro-scale λ_g^+ calculated from DNS simulations (——) from bottom to top at $Re_\tau = 550$ (present data), $Re_\tau = 1020$ [28] and $Re_\tau = 2004$ [29] and (- - - -) from the corresponding scaling $\lambda_g^+ = A\sqrt{\kappa y^+}$, where A is estimated in the range $80 < y+ < Re_\tau/5$, (*b*) y-dependence of the Taylor scale evaluated with relation (A.1) when the dimensional predictions of η and L_s are calculated via the profiles of $\langle\epsilon\rangle$ and S for the same DNS data sets.

expressions in equation (A.1) leads to a scaling function of the transverse Taylor micro-scale λ_g in terms of the wall distance,

$$\lambda_g^+ \approx A(\kappa y^+)^{1/2}, \tag{A.2}$$

where A is a constant which should approach a universal value in the limit of large Reynolds number. The assumptions made are the same as used in [22] where a similar scaling law for the Taylor micro-scale was proposed. If equation (A.2) holds, the wall-distance scaling of the transverse Taylor micro-scale definition, responsible for the span-wise resolution effects of the hot wire, should be

$$\frac{1}{2}\left(\frac{\partial^2 \rho_{11}}{\partial r_3^2}\right)^+_{\mathbf{x_0}} \approx -\frac{1}{A^2(\kappa y^+)}. \tag{A.3}$$

Relation (A.2) is shown in figure A1(*a*) together with different DNS data set with Re_τ from 550 to 2004 [28, 29]. The proposed scaling shows fairly good agreement in the region $80 < y^+ < Re_\tau/5$. However, the asymptotic features of the equilibrium range are certainly not reached with the present Reynolds number data sets, as confirmed by the increasing value of λ_g^+ at a given location with the friction Reynolds number. Indeed, in figure A1(*b*), the y-dependence of the Taylor scale evaluated with relation (A.1), when the dimensional predictions of η and L_s are calculated via the profiles of $\langle\epsilon\rangle$ and S, exhibits the same qualitative trend. In detail, the deviation from the expected $y^{1/2}$ behavior seems to decrease moving to a larger Reynolds number data set with an increasing value of λ_g.

References

[1] Marusic I, Uddin A K M and Perry A E 1997 Similarity law for the streamwise turbulence intensity in zero-pressure-gradient turbulent boundary layers *Phys. Fluids* **9** 3718–26

[2] Marusic I and Kunkel G J 2003 Streamwise turbulence intensity formulation for flat-plate boundary layers *Phys. Fluids* **15** 2461–4

[3] Talamelli A, Persiani F, Fransson J H M, Alfredsson P H, Johansson A V, Nagib H M, Rüedi J-D, Sreenivasan K R and Monkewitz P A 2009 CICLoPE—a response to the need for high Reynolds number experiments *Fluid Dyn. Res.* **41** 021407

[4] Örlü R, Hutchins N, Kurian T and Talamelli A 2009 Challenges in hot wire measurements in wall-bounded turbulent flows *Bulletin of the American Physical Society, 62nd Annual Meeting of the APS Division of Fluid Dynamics, (Minneapolis, MN, 22–24 November, 2009)* vol 54

[5] Marusic I, McKeon B J, Monkewitz P A and Nagib H M 2010 Wall-bounded turbulent flows at high Reynolds numbers: recent advances and key issues *Phys. Fluids* **22** 065103

[6] Talamelli A, Westin K J A and Alfredsson P H 2000 An experimental investigation of the response of hot-wire x-probes in shear flows *Exp. Fluids* **28** 425–35

[7] Cutler A D and Bradshaw P 1991 A crossed hot-wire technique for complex turbulent flows *Exp. Fluids* **12** 17–22

[8] Bayley S C C, Kunkel G J, Hultmark M, Vallikivi M, Hill J P, Meyer K A, Tsay C, Arnold C B and Smits A J 2010 Turbulence measurements using a nanoscale thermal anemometry probe *J. Fluid Mech.* **663** 160

[9] Frenkiel F N 1949 The influence of the length of a hot wire on the measurements of turbulence *Phys. Rev.* **75** 1263–4

[10] Ligrani P M and Bradshaw P 1987 Spatial resolution and measurement of turbulence in the viscous sublayer using subminiature hot-wire probes *Exp. Fluids* **5** 407–17

[11] Alfredsson P H, Johansson A V, Haritonidis J H and Eckelmann H 1988 The fluctuating wall-shear stress and the velocity field in the viscous sublayer *Phys. Fluids* **31** 1026–33

[12] Örlü R and Alfredsson P H 2010 On spatial resolution issues related to time-averaged quantities using hot-wire anemometry *Exp. Fluids* **49** 101–10

[13] Monkewitz P A, Duncan R D and Nagib H M 2010 Correcting hot-wire measurements of stream-wise turbulence intensity in boundary layers *Phys. Fluids* **22** 091701

[14] Suzuki Y and Kasagi N 1992 Evaluation of hot-wire measurements in wall shear turbulence using a direct numerical simulation database *Exp. Therm. Fluid Sci.* **5** 69–77

[15] Hutchins N, Nickels T B, Marusic I and Chong M S 2009 Hot-wire spatial resolution issues in wall-bounded turbulence *J. Fluid Mech.* **635** 103–36

[16] Chin C C, Hutchins N, Ooi A S H and Marusic I 2009 Use of direct numerical simulation (DNS) data to investigate spatial resolution issues in measurements of wall-bounded turbulence *Meas. Sci. Technol.* **20** 115401

[17] Smits A J, Monty J, Hultmark M, Bailey S C C, Hutchins N and Marusic I 2011 Spatial resolution correction for wall-bounded turbulence measurements *J. Fluid Mech.* **676** 41–53

[18] Bruun H H 1995 *Hot-Wire Anemometry: Principles and Signal Analysis* (Oxford: Oxford University Press)

[19] Lundbladh A, Henningson D S and Johansson A V 1992 An efficient spectral integration method for the solution of the Navier–Stokes equations *Technical Report* FFA-TN-28, Aeronautical Research Institute of Sweden, Department of mechanics KTH

[20] Johansson A V and Alfredsson P H 1983 Effects of imperfect spatial resolution on measurements of wall-bounded turbulent shear flows *J. Fluid Mech.* **137** 409–21

[21] Tennekes H and Lumley J L 1997 *A First Course in Turbulence* (Cambridge, MA: MIT Press)

[22] Blair M F and Bennet J C 1987 Hot-wire measurements of velocity and temperature fluctuations in a heated turbulent boundary layer *J. Phys. E: Sci. Instrum.* **20** 209–16

[23] Hallbäck M, Groth J and Johansson A V 1989 A Reynolds stress closure for the dissipation in anisotropic turbulent flows *Proc. 7th Symp. on Turbulent Shear Flows (Stanford, CA, 21–23 August)* vol 2 (University Park, PA: Pennsylvania State University) pp 17.2.1–6

[24] Segalini A, Örlü R, Schlatter P, Alfredsson P H, Rüedi J-D and Talamelli A 2011 A method to estimate turbulence intensity and transverse Taylor microscale in turbulent flows from spatially averaged hot-wire data *Exp. Fluids* **51** 693–700

[25] Pope S B 2000 *Turbulent Flows* (Cambridge: Cambridge University Press)

[26] Casciola C M, Gualtieri P, Jacob B and Piva R 2007 The residual anisotropy at small scales in high shear turbulence *Phys. Fluids* **19** 101704

[27] Cimarelli A and De Angelis E 2011 Analysis of the Kolmogorov equation for filtered wall turbulent flows *J. Fluid Mech.* **676** 367–95

[28] del Alamo J C, Jiménez J, Zandonade P and Moser R D 2004 Scaling of the energy spectra of turbulent channels *J. Fluid Mech.* **500** 135–44

[29] Hoyas S and Jiménez J 2006 Scaling of the velocity fluctuations in turbulent channels up to $Re_\tau = 2003$ *Phys. Fluids* **18** 011702